Electro-Flow Focusing: The High-Conductivity Low-Viscosity Limit

Alfonso M. Gañán-Calvo*

Escuela Superior de Ingenieros, Universidad de Sevilla, Camino de los Descubrimientos, 41092 Sevilla, Spain

(Received 28 July 2006; revised manuscript received 6 February 2007; published 30 March 2007)

Electro-flow focusing, a technique combining the features of electrospray (ES) and flow focusing (FF), provides a reliable tool to reach parametrical microjetting ranges not attainable by ES or FF alone under specific operational regimes (liquid properties and flow rate). In this Letter, we provide not only a closed theoretical model predicting the diameter of a high electrical conductivity electro-flow focused liquid microjet, but also its convective or absolute instability, linked to the jetting-to-dripping transition and the minimum liquid flow rate that can be ejected in steady jetting regime, in which the smallest droplets are issued. Good agreement is found with experimental values.

DOI: 10.1103/PhysRevLett.98.134503 PACS numbers: 47.55.D−, 47.20.Dr, 47.55.db, 47.65.−d

Owing to extensive technological applications, on the track of pioneers [1,2], the physics of cone-jet electrospray has come under intense scrutiny in the last decades ([3–9], among others). In addition, flow focusing [10,11] has earned attention in the microfluidic community owing to its simplicity, robustness, and reliability as a means to generate steady microjets and nearly monodisperse microdroplets. Numerous applications exist, e.g., the production of high quality aerosols and microspheres [12]. The combination of electrospray and flow focusing (electro-flow focusing [13], EFF; see Fig. 1), an alternative to either technique on its own, is here analyzed in the limits of high electrical conductivity of the focused liquid, and low viscosities of both focused and focusing fluids. For any particular choice of fluid properties and flow rates, EFF leads to extended microjetting parametrical ranges, and therefore to thinner and faster microjets whose final diameter is here theoretically predicted. Our analysis is particularly well suited for high-conductivity aqueous solutions and liquid metals focused by other dielectric fluids (gases or liquids, [14]). Further model developments could explore the influence of other parameters: moderate viscosity, bulk free charge relaxation, or polarization forces.

Thus, a plurality of theoretical insights are here brought together, including free-surface inviscid electrohydrodynamic flow, and spatiotemporal stability analysis. In effect, we examine the parametrical ranges where electro-flow focused steady jets can be achieved in the low-viscosity range. The convective-absolute (CA) instability boundary obtained is assumed coincident with the jetting-to-dripping transition; it is located at the minimum flow rate that can be steadily electro-flow focused (as observed in electrospray). Our model includes the key physical parameters acting on the CA transition in a wide range of situations. We consider liquids of low viscosity and high electrical conductivity, e.g., aqueous solutions and liquid metals, focused by low-viscosity dielectric fluids. In addition, interfacial boundary layer effects are taken into account, revealing their influence on the jet instability.

Theoretical model. Steady jet diameter.—A flow rate Q_1 of a liquid of density ρ_1 and small viscosity μ_1, with good electrical conductivity, is ejected into the ambient through a small orifice of radius R, in the form of a liquid jet of radius $R_o \ll R$ issuing from a large meniscus (see Fig. 1 and [10]). A flow rate Q_2 of a second dielectric fluid of density ρ_2 and small viscosity μ_2 is forced coaxially with the liquid conductor through the round exit orifice. The 1–2 interface is maintained at a constant electric voltage V (tangential electric field along the jet surface vanishes) relative to the orifice plate. Neglecting the boundary layer thickness at the orifice edge and the influence of the thin focused jet, the fluid velocity near the axis at the exit orifice can be equated to the inviscid velocity ([15], p. 1294):

$$U_2 = \frac{Q_2}{2\pi R^2}. \tag{1}$$

In addition, since the normal electric field at the jet surface (E_n) is much larger than the one at the upstream meniscus surface (Fig. 1 [6]), the following momentum balance holds at the orifice exit:

$$2\sigma R_o^{-1} + \rho_1\left(\frac{Q_1}{\pi R_o}\right)^2 = \varepsilon_o E_n^2 + \rho_2\left(\frac{Q_2}{2\pi R}\right)^2 \tag{2}$$

(surface tension σ, vacuum permittivity ε_o). Dividing Eq. (2) by $\rho_1(\frac{Q_1}{\pi R_o})^2$ leads to

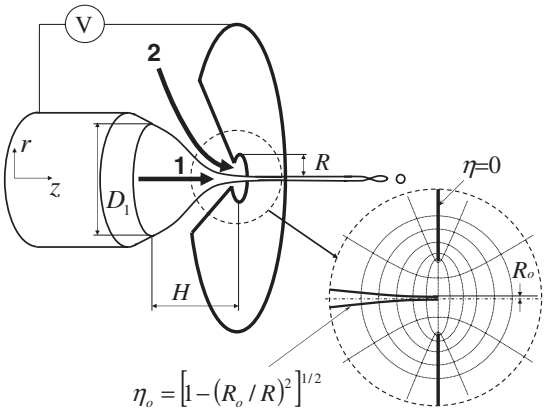

FIG. 1. The electro-flow focusing (EFF) configuration. Oblate spheroidal coordinates.

$$\Gamma = \frac{2}{\mathrm{We}} + 1 - \frac{1}{4}\rho Q^2 x^4, \tag{3}$$

where $x = R_o/R$, $\rho = \rho_2/\rho_1$, and $Q = Q_2/Q_1$. $\mathrm{We} = \rho_1 Q_1^2(\pi^2 R_o^3\sigma)^{-1}$ is the Weber number and $\Gamma = \pi^2\varepsilon_o E_n^2 R_o^4(\rho_1 Q_1^2)^{-1}$ is the nondimensional jet surface charge (squared).

Corona or gas ionization effects as well as ion evaporation kinetics at the vicinity of the exit orifice, either at the orifice edge or at the jet surface, will be ignored by our theory [16]. Now, the jet surface charge at the orifice may be accurately calculated by using the jet's geometry near the exit (Fig. 1). Oblate spheroidal coordinates (OSC) (η, ξ) provide an adequate basis for the description of the inviscid liquid flow and the electric field distribution upstream from the circular outlet (radius R). The expression of the jet's surface at the orifice in OSC is thus $\eta_o \simeq 1 - x^2/2$, as long as $x \ll 1$. The electrostatic field produced by the slender jet can be approximated by the wire-orifice field given by [17]:

$$\Psi(\eta,\xi) \simeq V\frac{\operatorname{arctanh}\eta}{\operatorname{arctanh}\eta_o} \longrightarrow E_n = -\frac{1}{h_\eta}\frac{\partial\Psi}{\partial\eta} \equiv -\frac{(1-\eta^2)^{1/2}}{\eta}\frac{\partial\Psi}{\partial\eta}, \tag{4}$$

where h_η is the scale factor of coordinate η. Thus, the dimensionless jet surface charge at the orifice exit can be approximated by

$$\Gamma = \pi^2\varepsilon_o E_n^2 R_o^4(\rho_1 Q_1^2)^{-1} \simeq \frac{\pi^2 x^2\varepsilon_o R^2 V^2}{\rho_1 Q_1^2[\ln(x/2)]^2}, \tag{5}$$

up to $O(x^2)$ errors, which combined with Eq. (3) and the (We, x, Q, ρ) definitions yield the expression for the jet radius R_o at the orifice exit in terms of the experimental parameters.

Jet instability. Derivation of the dispersion relation and parametrical realm of jetting.—The spatiotemporal (CA) instability of liquid jets has been the subject of increasing attention since pioneering works [18,19]; see also [11,20,21]. Assuming inviscid liquid flow, Leib and Goldstein determined the minimum liquid velocity below which a cylindrical jet becomes absolutely unstable. At that point, jet experiments show a transition from jetting to dripping, under similar operational conditions. To investigate the CA instability of the issuing charged jet, we assume: (1) the liquid meniscus from which the jet issues is stable; (2) the jet is sufficiently slender for the infinite cylinder theory to hold at the vicinity of the orifice exit. Assumption (1) involves setting the appropriate feeding tube–orifice distance H to ensure meniscus stability (see [22] for the purely electrostatic case, and [23] for a purely hydrodynamic example): therefore, our stability analysis will be limited to the study of the CA instability of the issuing liquid jet. We therefore study the spatiotemporal stability of an infinite cylindrical liquid jet with radius R_o, moving with uniform velocity U_1 surrounded by a coflowing stream of fluid 2 with uniform velocity U_2. U_1 and U_2 will generally be different, so that our model will be asymptotically correct if and only if viscous effects are consistently considered, confined to the vicinity of the interface. Evaluating the actual surface velocity U_s [24] is of fundamental importance in our spatiotemporal instability analysis since the effect of the convective velocity on surface waves cannot be neglected. Thus, viscous effects are only noticeable in two adjoining boundary layers whose thicknesses are $\delta_1 \sim (\mu_1 R R_o^2\rho_1^{-1}Q_1^{-1})^{1/2}$ and $\delta_2 \sim (\mu_2 R^3\rho_2^{-1}Q_2^{-1})^{1/2}$. Axial pressure gradients are moderate enough along the jet surface ($R_o \ll R$) to ensure that almost-Blasius layers develop simultaneously from the meniscus, provided $\delta_1 \ll R_o$ and $\delta_2 \ll R_o$. Thus, equating the viscous tangential stresses τ_1 and τ_2 at the jet surface, one obtains at the exit orifice:

$$[\mu_1\rho_1(U_s - U_1)^3]^{1/2} = [\mu_2\rho_2(U_2 - U_s)^3]^{1/2} \tag{6}$$

where U_1 and U_2 are naturally the axial velocities of the core liquid and the focusing fluid away from the boundary layers. This balance immediately provides an expression for U_s, given that $U_1 = Q_1/(\pi R_o^2)$ and $U_2 = Q_2/(2\pi R^2)$:

$$U_s = \left(\frac{1 + (\rho\mu)^{1/3}U_2/U_1}{1 + (\rho\mu)^{1/3}}\right)U_1 = \left(\frac{1 + (\rho\mu)^{1/3}Qx^2/2}{1 + (\rho\mu)^{1/3}}\right)\frac{Q_1}{\pi R_o^2} \tag{7}$$

where $\mu = \mu_2/\mu_1$. We use cylindrical polar coordinates (r, z) along the jet, and assume perturbations proportional to $\exp[i(kz - \omega t)]$. Wave frequency ω, time t, wave number k and coordinates $\{r, z\}$ are scaled with U_1/R_o, R_o/U_1, $1/R_o$, and R_o, respectively. In our analysis, we assume the liquid to be an inviscid perfect conductor. The equations expressing mass, momentum, and electric charge conservation for both fluids 1 (conductor) and 2 (dielectric), together with the normal stress balance at the jet surface (see, for example, [25] for a simple derivation without dynamic effects of the outer dielectric), provide the dispersion relation between the wave number k and its corresponding frequency ω. In our spatiotemporal analysis, since the liquid moves with uniform velocity U_1, we need to replace the wave frequency ω by $\omega' = (\omega - k)$ in the dispersion relation. Furthermore, while in [25] the electric field is caused by a given voltage difference between the jet and a concentric electrode of radius b, the surface charge Γ is here related to the applied voltage V through Eq. (5). Accordingly, the following asymptotically consistent dispersion relation results:

$$(\omega - k)\left(\omega - k\frac{U_s}{U_1}\right)\frac{I_o(k)}{I_1(k)} + \rho\left(\omega - k\frac{U_s}{U_1}\right)\left(\omega - k\frac{U_2}{U_1}\right)\frac{K_o(k)}{K_1(k)} = \left\{\frac{(k^2-1)}{\mathrm{We}} + \Gamma\left[1 - k\frac{K_1(k)}{K_o(k)}\right]\right\}k \tag{8}$$

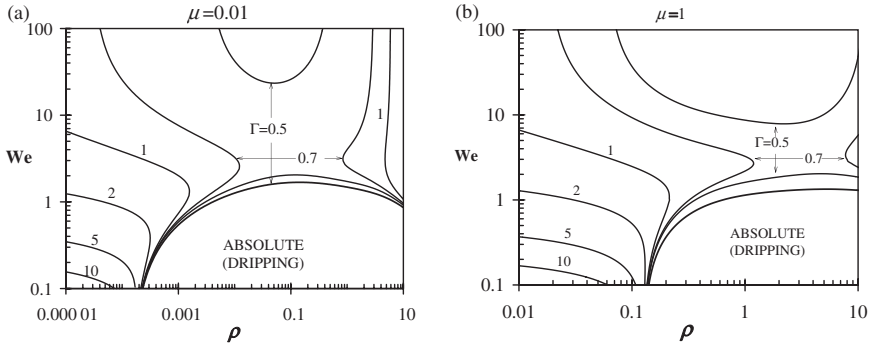

FIG. 2. Isocontours of the CA transition surface {We, Γ, ρ, μ}. (a) $\mu = 0.01$; (b) $\mu = 1$.

where both ω and k are assumed complex numbers; I and K are Bessel functions. Next, we follow a spatiotemporal formalism to describe the CA character of axisymmetric instabilities in the four-dimensional space {We, Γ, ρ, μ}. We seek solutions of the dispersion relation 8 which satisfy $d\omega/dk = 0$ and sit in the lower complex half plane $\mathrm{Im}(k) < 0$, with $\mathrm{Im}(\omega) \geq 0$ [18,26–29]. We choose solutions whose spatial branches departing from the saddle point $d\omega/dk = 0$ originate from separate halves of the k plane ([28], p. 484).

Although an exhaustive exploration of the parametrical realm {We, Γ, ρ, μ} is here out of our scope, a significant collection of results are summarized in Figs. 2(a) and 2(b), where we have plotted by contour lines the CA transition surface $\Gamma = \Gamma(\mathrm{We}, \rho; \mu)$ for $\mu = 0.1$ and $\mu = 1$ below (above) which the instability is convective (absolute). The values of ρ and μ explored correspond to common solvents and liquid metals EFF focused by any gas o common liquid dielectric (e.g., water in air, water in oil [30], mercury in octane). Interestingly, there is a Weber number range $\mathrm{We} = \mathrm{We}(\rho, \mu)$ where the instability is always absolute (unconditional dripping) independently of Γ. This area is marked below the $\Gamma = 0$ isocontour in Figs. 2(a) and 2(b). More interestingly, from the trends exhibited in these figures and making We sufficiently small, one can obtain the density ratio ρ as a function of μ below which unconditional convective instability (unconditional jetting) is found in the absence of electrification, see Fig. 3. For ρ values above that curve $\rho = \rho(\mu)$ in Fig. 3, one can find absolute or convective instability depending on We and Γ. This striking result has a clear physical explanation: those focusing fluids providing surface velocities $U_s/U_1 > 1$ above all upstream wave speeds (requiring smaller ρ with μ as large as possible) always pull jets from their focused partners. The location of nine fluid pairs in the (μ, ρ) plane is plotted: three liquid conductors (mercury, gallium, saline water) combined with three focusing dielectric fluids (air, heptane, silicone oil $\mu = 5$ cP). Only those combinations involving metals and focusing fluids with larger kinematic viscosities $\nu_2 = \mu_2/\rho_2$ (namely air $\nu_2 = 1.5 \times 10^{-5}$ m^2/s, and silicone oil $\nu_2 = 5.15 \times 10^{-6}$ m^2/s) lead to unconditional jetting in the absence of electrification, a result of practical importance.

Our CA predictions have been carefully tested by experiment. A pressurized aluminum cubic box (50 mm long, wall thickness 5 mm) with a 2 mm hole centered in one of its faces is used. A 3 mm disk (75 μm thick) with a central orifice (radius $R = 100$ μm) is glued to the inner side of the 2 mm hole and aligned with it, covering it completely. A stainless steel liquid feeding tube (OD 1 mm, ID 0.7 mm) passes through the opposite face of the box, and a 7 mm long silica capillary (sharpened as in Fig. 1, with $D_1 = 150$ μm) protrudes from its end inside the box. The tip of said silica capillary, coaxial with the orifice, is located at $H = 200$ μm from the 3 mm disk. Filtered drinking water (measured electrical conductivity $K \sim 0.015$ S/m, and surface tension $\sigma = 0.072$ N/m) is supplied through the tube by a Cole-Parmer pump (syringe B-D 20 cm^3), voltage by a power supply Bertan 250B-10R, and compressed air is supplied to the box at a constant flow rate $Q_2 = 23$ l/h (std). Here $\rho = 0.0012$ and $\mu = 0.016$. Transitional flow rates are carefully assessed by observation of the sudden issuing spray changes at the jetting-to-dripping

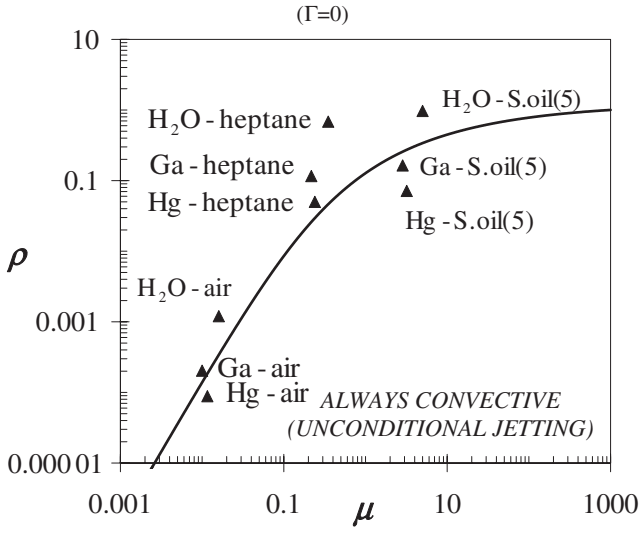

FIG. 3. Density ratio ρ values below which unconditional jetting is found: no electrification. Several fluid pairs shown: three liquid conductors (mercury, gallium, saline water) and three focusing dielectric fluids (air, heptane, silicone oil $\mu = 5$ cP).

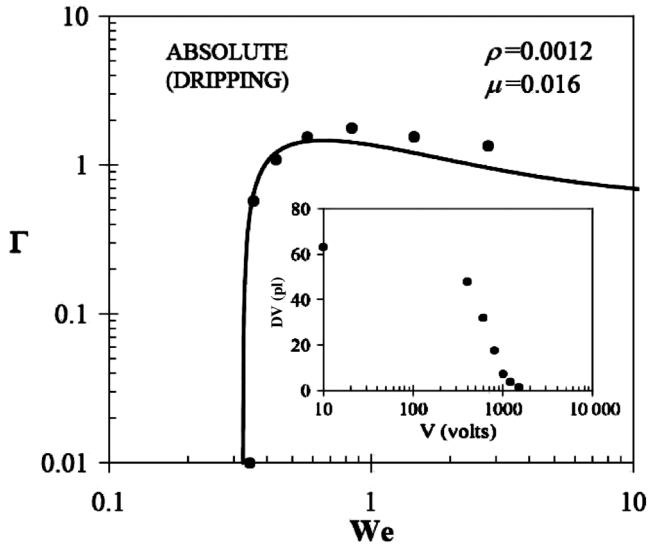

FIG. 4. Experimental (dots) vs theoretical (continuous line) Γ values of the CA transition as a function of We ($\rho = 0.0012$, $\mu = 0.016$). The inset gives the theoretical droplet volume DV in pl (jetting regime), as a function of the applied voltage; [30] shows a similar trend in a liquid-liquid experimental setup.

transition, thus obtaining the transition Q_1 as a function of applied voltage V, from which We and Γ are evaluated from Eqs. (3) and (5). Experimental agreement with theoretical predictions (Fig. 4) is good and promising: deviations occur only for $V > 1$ kV (We values above 0.8 in the plot), when tangential electric fields on the jet surge owing to finite conductivity effects, enhancing convective instability. A very significant droplet volume reduction obtained for increasing applied voltage in the jetting regime, close to the CA transition, is shown in Fig. 4 (inset). Experimentally measured droplet size values deviate from theoretical prediction [using Eqs. (3) and (5), and the instability wavelengths given by the stability analysis] less than 20%, within the jetting parametrical regime.

This work is supported by the Ministry of Science and Technology of Spain, Grant No. DPI2004-07197. The experimental measurements have been taken by Mr. Benjamin Bluth. Suggestions from Dr. Pascual Riesco-Chueca and extensive discussions with Dr. Piotr Garstecki are highly appreciated.

*Email address: amgc@us.es

[1] J. Zeleny, Phys. Rev. **10**, 1 (1917).
[2] G. I. Taylor, Proc. R. Soc. A **280**, 383 (1964).
[3] D. P. H. Smith, IEEE Trans. Ind. Appl. **22**, 527 (1986).
[4] M. Cloupeau and B. Prunet-Foch, J. Electrost. **22**, 135 (1989).
[5] L. Cherney, J. Fluid Mech. **378**, 167 (1999).
[6] A. M. Gañán-Calvo, Phys. Rev. Lett. **79**, 217 (1997).
[7] F. Higuera, J. Fluid Mech. **484**, 303 (2003).
[8] A. Barrero, J. López-Herrera, A. Boucard, I. Loscertales, and M. Marquez, J. Colloid Interface Sci. **272**, 104 (2004).
[9] J. F. de la Mora, Annu. Rev. Fluid Mech. **39**, 217 (2007).
[10] A. M. Gañán-Calvo, Phys. Rev. Lett. **80**, 285 (1998).
[11] A. M. Gañán-Calvo and P. Riesco-Chueca, J. Fluid Mech. **553**, 75 (2006).
[12] L. Martín-Banderas, M. Flores-Mosquera, P. Riesco-Chueca, A. Rodríguez-Gil, A. Cebolla, S. Chávez, and A. M. Gañán-Calvo, Adv. Mater. **18**, 559 (2006).
[13] A. M. Gañán-Calvo, J. M. López-Herrera, and P. Riesco-Chueca, J. Fluid Mech. **566**, 421 (2006).
[14] A. M. Gañán-Calvo and J. M. López-Herrera, International Patent Application No. WO 03/066231, A1 (2003).
[15] P. M. Morse and H. Feshback, *Methods of Theoretical Physics* (McGraw-Hill Pub. Co., New York, 1953).
[16] These effects may occur very close and downstream the orifice exit plane, when the normal electric field on the jet E_n overcomes a certain threshold; currently under discussion [13].
[17] Analytical conjugate of the gas velocity potential for the flow through a round orifice [15].
[18] S. J. Leib and M. E. Goldstein, J. Fluid Mech. **168**, 479 (1986).
[19] S. J. Leib and M. E. Goldstein, Phys. Fluids **29**, 952 (1986).
[20] S. P. Lin and Z. W. Lian, Phys. Fluids A **5**, 771 (1993).
[21] S. P. Lin, *Breakup of Liquid Sheets and Jets* (Cambridge University Press, Cambridge, U.K., 2003).
[22] C. Pantano, A. M. Gañán-Calvo, and A. Barrero, J. Aerosol Sci. **25**, 1065 (1994).
[23] W. W. Zhang, Phys. Rev. Lett. **93**, 184502 (2004); S. Courrech du Pont and J. Eggers, Phys. Rev. Lett. **96**, 034501 (2006).
[24] J. M. Gordillo, M. Pérez-Saborid, and A. M. Gañán-Calvo, J. Fluid Mech. **448**, 23 (2001).
[25] E. R. Setiawan and S. D. Heister, J. Electrost. **42**, 243 (1997).
[26] R. J. Briggs, *Electron-Stream Interaction with Plasmas* (MIT Press, Cambridge, MA, 1961).
[27] J. B. Keller, S. L. Rubinov, and Y. O. Tu, Phys. Fluids **16**, 2052 (1973).
[28] P. Huerre and P. A. Monkewitz, Annu. Rev. Fluid Mech. **22**, 473 (1990).
[29] J. M. Chomaz, Annu. Rev. Fluid Mech. **37**, 357 (2005).
[30] D. R. Link, E. Grasland-Mongrain, A. Duri, F. Sarrazin, Z. Cheng, G. Cristobal, M. Marquez, and D. A. Weitz, Angew. Chem., Int. Ed. **45**, 2556 (2006).